CHIN. PHYS. LETT. Vol. 34, No. 11 (2017) 117201

New Method for 3D Transient Eddy Current Field Calculation and Its Application in Magneto-Acoustic Tomography *

Yuan-Yuan Li(李元园)[1,2], Guo-Qiang Liu(刘国强)[1,2**], Hui-Xia(夏慧)[1**], Li-Li Hu(胡丽丽)[1]

[1]*Institute of Electrical Engineering, Chinese Academy of Sciences, Beijing 100190*

[2]*University of Chinese Academy of Sciences, Beijing 100190*

(Received 3 May 2017)

A new method of 3D transient eddy current field calculation is proposed. The Maxwell equations with time component elimination (METCE) are derived under the assumption of magnetic quasi static approximation, especially for the sample of low conductivity. Based on METCE, we deduce a more efficient reconstruction algorithm of a 3D transient eddy current field. The computational burden is greatly reduced through the new algorithm, and the computational efficiency is improved. This new algorithm decompounds the space-time variables into two individual variables. The idea is to solve the spatial vector component firstly, and then multiply it by the corresponded time component. The iterative methods based on METCE are introduced to recover the distribution of conductivity in magneto-acoustic tomography. The reconstructed images of conductivity are consistent with the original distribution, which validate the new method.

PACS: 72.55.+s, 43.35.Rw, 41.20.Cv, 87.57.nf DOI: 10.1088/0256-307X/34/11/117201

In the field of geophysical exploration and biomedical engineering, many methods such as the transient electromagnetic method,[1−3] magneto-acoustic tomography[4−12] and magneto-acousto-electrical tomography[13−22] have been proposed. All the methods mentioned above are concerned with models in which eddy currents are generated by the transient electromagnetic stimulation. The distribution of conductivity of the sample can be reconstructed in the mentioned methods, and the process demands hat the 3D eddy current field is calculated in each iteration. The method of $A-\varphi$ is a traditional way to calculate eddy currents, which has the advantage of high precision. The formulation of the method of $A-\varphi$ uses the magnetic vector potential $\tilde{\boldsymbol{A}}(\boldsymbol{r},t)$ in both the eddy current region and free of eddy current, and the electric scalar potential $\tilde{\varphi}(\boldsymbol{r},t)$ in eddy current region[23] (the tilde above a variable indicates that the corresponding variable is a function of both time and space). In recent years, the $A-\varphi$ method was improved by some researchers, e.g., Lin and Li introduced the time-stepping finite-element and boundary-element coupling method to reduce the subdivision of the grid of the surface between the eddy currents and free of eddy currents.[24] The method of $A-\varphi$ and the improved methods[24,25] could complete the iterations in the reconstructed process, while it creates the computational burden[26−28] which fails to achieve rapid reconstruction. In this study, a new method is introduced to overcome this difficulty, and the new method is validated by magneto-acoustic tomography.

Magneto-acoustic tomography which combines the merits of high contrast of electrical impedance tomography and high spatial resolution of sonography has been rapidly developed in recent years. In magneto-acoustic tomography, a transient electromagnetic field is applied to generate eddy currents in the sample. In the presence of a static magnetic field, the sample will vibrate due to the Lorentz force and then emit ultrasonic waves.[5−12] The ultrasonic signals are related to the conductivity of the sample, and the distribution of conductivity within the sample can be reconstructed from the measured ultrasonic signal. In the reconstructed process, the iterative calculation of the 3D eddy current field is needed.

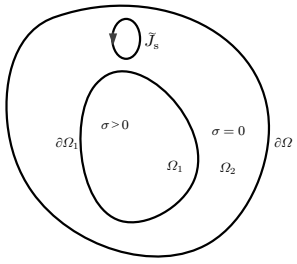

Fig. 1. Diagram of a sample of areas with and without eddy currents.

A typical eddy current problem is depicted in Fig. 1. It consists of an eddy current region Ω_1 with the conductivity of σ and a surrounding region free of eddy currents Ω_2, which contains the source of current $\tilde{\boldsymbol{J}}_{\rm s}(\boldsymbol{r},t)$. The entire problem region is denoted by Ω, and $\partial\Omega$ is the infinite boundary. The boundary of eddy currents and non-eddy currents region are $\partial\Omega_1$, and $\partial\Omega_2 = \partial\Omega_1 + \partial\Omega$, respectively. The

*Supported by the National Natural Science Foundation of China under Grant Nos 51137004, 61427806 and 51577184, and the Equipment Development Project of Chinese Academy of Sciences under Grant No YZ201507.

**Corresponding author. Email: gqliu@mail.iee.ac.cn; xiahui@mail.iee.ac.cn

© 2017 Chinese Physical Society and IOP Publishing Ltd

source of transient excitation applied to the coil is $\tilde{\boldsymbol{J}}_{\rm s}(\boldsymbol{r},t) = \boldsymbol{J}_{\rm s}(\boldsymbol{r})s(t)$, where $s(t)$ represents the time-varying term.

The primary magnetic field intensity $\tilde{\boldsymbol{H}}_1(\boldsymbol{r},t)$ satisfies Ampere's law, in Ω_2,

$$\nabla \times \tilde{\boldsymbol{H}}_1(\boldsymbol{r},t) = \tilde{\boldsymbol{J}}_{\rm s}(\boldsymbol{r},t). \tag{1}$$

The waveform of the primary magnetic intensity $\tilde{\boldsymbol{H}}_1(\boldsymbol{r},t)$ is the same of the source of transient excitation $\tilde{\boldsymbol{J}}_{\rm s}(\boldsymbol{r},t)$ as shown in Eq. (1). Thus the primary magnetic field intensity can be expressed as $\tilde{\boldsymbol{H}}_1(\boldsymbol{r},t) = \boldsymbol{H}_1(\boldsymbol{r})s(t)$, and the primary magnetic flux density can be expressed as $\tilde{\boldsymbol{B}}_1(\boldsymbol{r},t) = \tilde{\boldsymbol{B}}_1(\boldsymbol{r})s(t)$.

The displacement current is a minterm, which could be ignored under the assumption of magnetic quasi-static approximation in Ω_1. Thus the secondary magnetic field intensity satisfies

$$\nabla \times \tilde{\boldsymbol{H}}_2(\boldsymbol{r},t) = \sigma\tilde{\boldsymbol{E}}(r,t) + \frac{\partial\tilde{\boldsymbol{D}}(r,t)}{\partial t} \approx \sigma\tilde{\boldsymbol{E}}(r,t). \tag{2}$$

Considering that the conductivity of the medium is low in Ω_1, we can obtain that $|\tilde{\boldsymbol{H}}_2(\boldsymbol{r},t)|$ is much smaller than $|\tilde{\boldsymbol{H}}_1(\boldsymbol{r},t)|$, $|\tilde{\boldsymbol{H}}_2(\boldsymbol{r},t)| \ll |\tilde{\boldsymbol{H}}_1(\boldsymbol{r},t)|$. Therefore, the influence of $|\tilde{\boldsymbol{H}}_2(\boldsymbol{r},t)|$ could be ignored when calculating the induced electrical field intensity $\tilde{\boldsymbol{E}}(r,t)$ in Ω_1. According to Faraday's law of electromagnetic induction, the following equation can be estimated,

$$\begin{aligned}\nabla \times \tilde{\boldsymbol{E}}(\boldsymbol{r},t) &= -\frac{\partial\tilde{\boldsymbol{B}}(\boldsymbol{r},t)}{\partial t} \approx -\frac{\partial\tilde{\boldsymbol{B}}_1(\boldsymbol{r},t)}{\partial t} \\ &= -\boldsymbol{B}_1(\boldsymbol{r})g(t),\end{aligned} \tag{3}$$

where $g(t) = \frac{ds(t)}{dt}$, and the induced electrical field intensity $\tilde{\boldsymbol{E}}(r,t)$ has the same waveform of the time derivative of $\tilde{\boldsymbol{B}}_1(\boldsymbol{r},t)$, therefore $\tilde{\boldsymbol{E}}(r,t)$ can be expressed as $\tilde{\boldsymbol{E}}(\boldsymbol{r},t) = \boldsymbol{E}(\boldsymbol{r})g(t)$. Furthermore, according to Ohm's law, the induced current density $\tilde{\boldsymbol{J}}(\boldsymbol{r},t)$ can be expressed as $\tilde{\boldsymbol{J}}(\boldsymbol{r},t) = \sigma\tilde{\boldsymbol{E}}(\boldsymbol{r},t)$, as a consequence, the waveform of $\tilde{\boldsymbol{J}}(\boldsymbol{r},t)$ is the same as that of $\tilde{\boldsymbol{E}}(r,t)$ in Ω_1, i.e., $\tilde{\boldsymbol{J}}(\boldsymbol{r},t) = \boldsymbol{J}(\boldsymbol{r})g(t)$.

All the above states can be summarized as

$$\nabla \times \tilde{\boldsymbol{H}}_1(\boldsymbol{r},t) = \nabla \times (\boldsymbol{H}_1(\boldsymbol{r})s(t)) = \boldsymbol{J}_{\rm s}(\boldsymbol{r})s(t), \tag{4a}$$

$$\begin{aligned}\nabla \times \tilde{\boldsymbol{E}}(\boldsymbol{r},t) &= \nabla \times (\boldsymbol{E}(\boldsymbol{r})g(t)) \\ &\approx -\frac{\partial\tilde{\boldsymbol{B}}_1(\boldsymbol{r},t)}{\partial t} = -\boldsymbol{B}_1(\boldsymbol{r})g(t),\end{aligned} \tag{4b}$$

$$\begin{aligned}\nabla \cdot \tilde{\boldsymbol{B}}(\boldsymbol{r},t) &\approx \nabla \cdot \tilde{\boldsymbol{B}}_1(\boldsymbol{r},t) = \nabla \cdot (\boldsymbol{B}_1(\boldsymbol{r})s(t)) \\ &= \nabla \cdot (\boldsymbol{B}_1(\boldsymbol{r}))s(t) = 0,\end{aligned} \tag{4c}$$

$$\nabla \cdot \tilde{\boldsymbol{J}}(\boldsymbol{r},t) = \nabla \cdot (\sigma E(\boldsymbol{r},t)) = 0. \tag{4d}$$

The Maxwell equations with time component elimination (METCE) are obtained by eliminating the time components on both sides of Eq. (4),

$$\nabla \times \boldsymbol{H}_1(\boldsymbol{r}) = \boldsymbol{J}_{\rm s}(\boldsymbol{r}), \tag{5a}$$

$$\nabla \times \boldsymbol{E}(\boldsymbol{r}) = -\boldsymbol{B}_1(\boldsymbol{r}), \tag{5b}$$

$$\nabla \cdot \boldsymbol{B}_1(\boldsymbol{r}) = 0, \tag{5c}$$

$$\nabla \cdot \boldsymbol{J}(\boldsymbol{r}) = 0, \tag{5d}$$

where $\boldsymbol{E}(\boldsymbol{r})$ is the spatial component of the induced electrical field intensity, $\boldsymbol{H}_1(\boldsymbol{r})$ is the spatial component of the primary magnetic field intensity, $\boldsymbol{B}_1(\boldsymbol{r})$ is the spatial component of the primary magnetic flux density, $\boldsymbol{J}_{\rm s}(\boldsymbol{r})$ is the spatial component of the transient excitation, and $\boldsymbol{J}(\boldsymbol{r})$ is the spatial component of the induced current density.

Based on Eq. (5), a new method for the boundary value problem of the 3D model can be obtained; the differential equations and the boundary conditions are as follows: Eq. (5c) represents that the primary magnetic flux density $\boldsymbol{B}_1(\boldsymbol{r})$ can be expressed as

$$\boldsymbol{B}_1(\boldsymbol{r}) = \nabla \times \boldsymbol{A}_1(\boldsymbol{r}), \tag{6}$$

where $\boldsymbol{A}_1(\boldsymbol{r})$ is the spatial component of the primary magnetic vector potential corresponding to the spatial component of primary magnetic flux density $\boldsymbol{B}_1(\boldsymbol{r})$. The waveform of $\tilde{\boldsymbol{A}}_1(\boldsymbol{r},t)$ is similar to $\tilde{\boldsymbol{B}}_1(\boldsymbol{r},t)$ as shown in Eq. (6), $\tilde{\boldsymbol{A}}_1(\boldsymbol{r},t) = \boldsymbol{A}_1(\boldsymbol{r})s(t)$.

Substituting Eq. (6) into Eq. (5b) and introducing $\tilde{\varphi}(\boldsymbol{r},t) = \varphi(\boldsymbol{r})g(t)$ yield the electrical field intensity

$$\boldsymbol{E}(\boldsymbol{r}) = -\boldsymbol{A}_1(\boldsymbol{r}) - \nabla\varphi(\boldsymbol{r}), \tag{7}$$

where $\varphi(\boldsymbol{r})$ represents the spatial component of electric scalar potential. The form of Eq. (7) is different from the traditional $\tilde{\boldsymbol{E}}(r,t) = -\frac{\partial\boldsymbol{A}_1(r,t)}{\partial t} - \nabla\tilde{\varphi}(r,t)$. The reason is that the traditional one can be expressed as $\boldsymbol{E}(\boldsymbol{r})g(t) = -\boldsymbol{A}_1(\boldsymbol{r})g(t) - \nabla\varphi(\boldsymbol{r})g(t)$, then the time components can be eliminated, thus Eq. (7) is obtained.

Substituting Eq. (7) into Eq. (5d) yields

$$\nabla \cdot (\sigma\nabla\varphi(\boldsymbol{r})) = -\nabla \cdot (\sigma\boldsymbol{A}_1(\boldsymbol{r})). \tag{8}$$

The normal component of current density is zero on the boundary of $\partial\Omega_1$, namely

$$\boldsymbol{J}(\boldsymbol{r}) \cdot \boldsymbol{n}|_{\partial\Omega_1} = 0. \tag{9}$$

According to Eqs. (6)–(9) the new method for the boundary value problem of the 3D model is obtained in the form of

$$\nabla \cdot (\sigma\nabla\varphi(\boldsymbol{r})) = -\nabla \cdot (\sigma\boldsymbol{A}_1(\boldsymbol{r})), \tag{10a}$$

$$\left(\boldsymbol{A}_1(\boldsymbol{r}) \cdot \boldsymbol{n} + \frac{\partial\varphi(\boldsymbol{r})}{\partial n}\right)\Big|_{\partial\Omega_1} = 0. \tag{10b}$$

The new method significantly improves the calculation effectively. First, the solution region of Eq. (10) is reduced to the eddy current area rather than the areas with and without the eddy currents, which has been chosen as the solution region by the $A-\varphi$ method.

Secondly, the solved variables are decreased to only $\varphi(\boldsymbol{r})$ in Eq. (10), rather than $\tilde{\boldsymbol{A}}(\boldsymbol{r},t)$ and $\tilde{\varphi}(\boldsymbol{r},t)$ in $A-\varphi$. Therefore, the new algorithm can dramatically improve the reconstruction in magneto-acoustic tomography and well logging, in the fields of geophysical exploration and biomedical engineering.

Then the method is applied to magneto-acoustic tomography. In magneto-acoustic tomography, a sample is placed in a static magnetic field, while a transient electromagnetic field is applied to induce eddy currents in the sample. In the presence of a static magnetic field, the sample will vibrate due to the Lorentz force, and then will emit ultrasonic waves.[5–12] The generated acoustic pressure satisfies the equation[29,30]

$$\nabla^2 p - \frac{1}{c_{\rm s}^2}\frac{\partial^2 p}{\partial t^2} = \nabla\cdot(\boldsymbol{J}\times\boldsymbol{B}_0), \tag{11}$$

where $c_{\rm s}$ is the acoustic velocity in the sample, p is the acoustic pressure, J is the current density in the sample, and B_0 is the static magnetic field.

Using Green's function, the solution to Eq. (11) can be written as

$$p(\boldsymbol{r},t) = -\frac{1}{4\pi}\int_V d\boldsymbol{r}'\nabla\cdot(\boldsymbol{J}(\boldsymbol{r}')\times\boldsymbol{B}(\boldsymbol{r}'))\frac{\delta(t-\frac{R}{c_{\rm s}})}{R}, \tag{12}$$

where $R=|\boldsymbol{r}-\boldsymbol{r}'|$, and V represents the volume containing the acoustic source.

The ultrasonic signals are related to the conductivity of the sample, and the distribution of conductivity within the sample can be reconstructed from the measured ultrasonic signal. The reconstruction of conductivity from acoustic pressure takes two steps. In the first step, $\nabla\cdot(\boldsymbol{J}\times\boldsymbol{B}_0)$ is reconstructed from acoustic pressure by the method of time reversal,[31]

$$\nabla\cdot(\boldsymbol{J}\times\boldsymbol{B}_0) = -\frac{1}{2\pi c_{\rm s}^3}\int_V dS_{\rm d}\frac{\boldsymbol{n}\cdot(\boldsymbol{r}_{\rm d}-\boldsymbol{r})}{|\boldsymbol{r}_{\rm d}-\boldsymbol{r}|^2} \cdot p''(\boldsymbol{r}_{\rm d},|\boldsymbol{r}_{\rm d}-\boldsymbol{r}|/c_{\rm s}), \tag{13}$$

where $\boldsymbol{r}_{\rm d}$ is a point on the detection surface with the normal vector $\boldsymbol{n}$, and $\boldsymbol{r}$ is a point in the sample. The double prime on p means the second derivative against time.

In the second step, the conductivity distribution is reconstructed from $\nabla\cdot(\boldsymbol{J}\times\boldsymbol{B}_0)$. Reconstructing conductivity σ from $\nabla\cdot(\boldsymbol{J}\times\boldsymbol{B}_0)$ is a work of iteration.

We define the direction of the static magnetic field in the Z axis. Therefore, the left term $\nabla\cdot(\boldsymbol{J}\times\boldsymbol{B}_0) = \boldsymbol{B}_0\cdot\nabla\times\boldsymbol{J} - \boldsymbol{J}\cdot\nabla\times\boldsymbol{B}_0$ in Eq. (14) can be simplified to $\nabla\cdot(\boldsymbol{J}\times\boldsymbol{B}_0) = \boldsymbol{B}_0\cdot\nabla\times\boldsymbol{J}|_z$.

The induced current density $\boldsymbol{J}(\boldsymbol{r})$ is obtained based on Eq. (7),

$$\boldsymbol{J}(\boldsymbol{r}) = -\sigma\boldsymbol{A}_1(\boldsymbol{r}) - \sigma\nabla\varphi(\boldsymbol{r}). \tag{14}$$

Taking the curl operator of both sides of Eq. (14) and separating the z-component, we obtain

$$\nabla\times[\sigma\boldsymbol{A}_1(\boldsymbol{r}) + \sigma\nabla\varphi(\boldsymbol{r})]_z = -\nabla\times\boldsymbol{J}(\boldsymbol{r})|_{(x,y,z_0)}, \tag{15}$$

where z_0 is the coordinate of the Z axis of a cross section.

The iterations should be taken as the following three steps. (1) Solve the boundary value problem of Eq. (10) with any given distribution of conductivity σ_i, and then work out the $\varphi(\boldsymbol{r})_i$. (2) Substitute $\varphi(\boldsymbol{r})_i$ into Eqs. (14) and (15) by the method of finite-difference and refresh σ_i in each small region. Go back to Eq. (10) with new σ_i for refreshing $\varphi(\boldsymbol{r})$ and $\boldsymbol{J}(\boldsymbol{r})$. (3) Compare the obtained result of conductivity with the predefined errors. If the result is smaller than the predefined errors, the iteration should be terminated, otherwise go to step 1.

To invalidate the new method and to explore its application, we establish a series of simulations and compared the new method with the method of $A-\varphi$. The simulation model shown in Fig. 2 includes two parts: (1) a cube space Ω_2 to stimulate the background of a vacuum; (2) a small cylinder Ω_1 with conductivity of σ. The conductivity σ changes from 0.1 S/m to 100 S/m, in Ω_1, and the pulse width of $\tilde{\boldsymbol{J}}_{\rm s}(\boldsymbol{r},t)$ is a variable in the range of 0.52 μs to 124.8 μs.

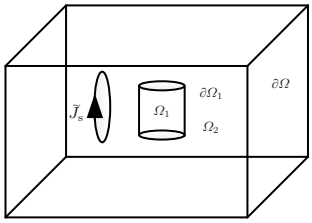

Fig. 2. Model of 3D cylindrical.

The error of electric scalar potential $\delta\varphi(\%)$ between $A-\varphi$ and the new algorithm, the conductivity of the sample, and the pulse width of the transient excitation are listed in Table 1. When the conductivity is below 10 S/m, the maximum and minimum errors of $\delta\varphi(\%)$ in Table 1 are 1.26% and 0.15%, respectively.

Table 1. The error of $\delta\varphi(\%)$.

Pulse width	0.1 (S/m)	1 (S/m)	10 (S/m)	100 (S/m)
0.52 μs	0.2851	0.6126	1.2632	7.2103
1.3 μs	0.25182	0.5659	1.1828	6.454267
5.2 μs	0.21144	0.5290	1.1486	5.765433
20.8 μs	0.18098	0.4103	0.9376	4.96306
124.8 μs	0.15073	0.3032	0.6647	2.434343

The error of magnetic vector potential $\delta A(\%)$, the conductivity of the sample, and the pulse width of the transient excitation are listed in Table 2. When the conductivity is below 10 S/m, the maximum and minimum errors of $\delta A(\%)$ in Table 2 are 0.7% and 0.00003%, respectively.

Table 2. The error of $\delta A(\%)$.

Pulse width	0.1 (S/m)	1 (S/m)	10 (S/m)	100 (S/m)	1000 (S/m)
0.52 μs	0.01756	0.07965	0.70122	7.3152	89.7215
1.3 μs	0.00955	0.04011	0.404639	3.94195	43.0548
5.2 μs	0.0025	0.00965	0.101114	1.01797	10.4148
20.8 μs	0.0002	0.00203	0.024886	0.25300	2.49147
124.8 μs	0.00003	0.00036	0.003725	0.04181	0.42146

The analysis of error demonstrates that the algorithm of Eq. (10) is valid in the application of low conductivity medium under magnetic quasi static approximation, especially for wider pulse width.

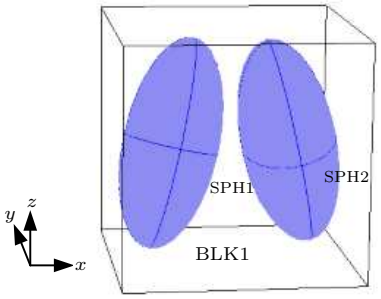

Fig. 3. Model of 3D ellipsoid.

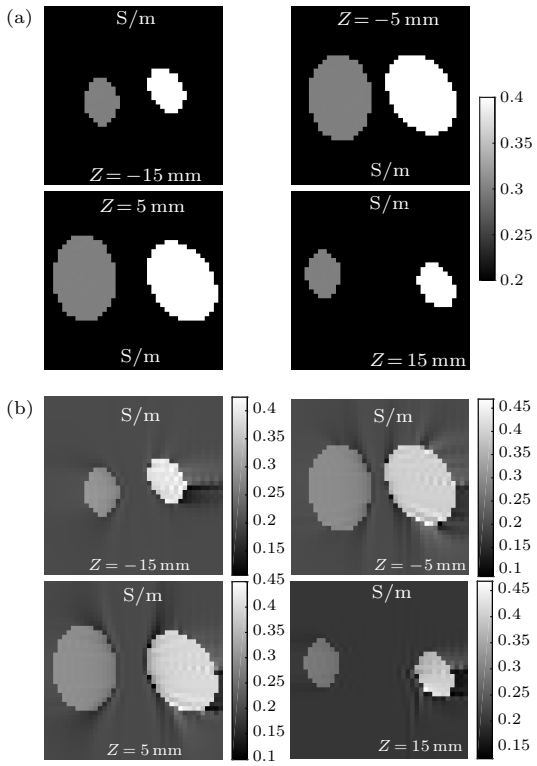

Fig. 4. The distribution of conductivity of different cross sections: (a) original conductivity, and (b) reconstructed conductivity.

Here a complex model is built as shown in Fig. 3. The conductivities of BLK1, SPH1, and SPH2 are 0.2 S/m, 0.3 S/m, and 0.4 S/m, respectively. Then we use Eqs. (13)–(15) to recover the distribution of conductivity in magneto-acoustic tomography, and the calculations of eddy currents are required in the step of every iteration.

The original conductivity of different cross sections is shown in Fig. 4(a), and the corresponding reconstructed conductivity is shown in Fig. 4(b). The relative errors between the original conductivity distribution and the reconstructed conductivity distribution are 2.72%, 2.13%, 2.23%, and 1.43%, respectively. Thus the reconstruction results are consistent with the original conductivity.

It can also be seen from the results that the reconstructed conductivity has gradual edges, which is different from the target distribution. This is caused by the limited number of sub-blocks of the reconstruction. Furthermore, the singularity of the conductivity gradient at the edge of the piecewise uniform conductivity introduces the image distortion at these locations. Although the proposed algorithms have some distortions, the results are still consistent with the original conductivity distribution.

In summary, we first derived Maxwell's equations with time components elimination under the magnetic quasi-static approximation, especially for a low conductivity medium. Based on these equations, a new algorithm to solve the problem of 3D transient eddy currents field is deduced. In the process of 3D conductivity reconstruction, we apply the new algorithm, which greatly reduces the computational burden and improves the efficiency of iteration. Although the reconstructed errors still exist, the reconstructed conductivity images are consistent with the original one. Compared with the traditional reconstructed methods, the new iteration method benefits from the rapid inversion and is convenient for the calculation. Therefore, the new algorithm has the prospect of applications in many fields such as geophysical exploration and biomedical engineering.

References

[1] Noda T 2008 *IEEE Trans. Power Delivery* **23** 1262
[2] Danielsen J E, Auken E, Jørgensen F, Søndergaard V and Sørensen K I 2003 *J. Appl. Geophys.* **53** 181
[3] Wu G J, Shen C Y, Tan H B and Yang G L 2016 *Acta Seismol. Sin.* **29** 235
[4] Li X and He B 2010 *IEEE Trans. Med. Imaging* **29** 1759
[5] Xu Y and He B 2005 *Phys. Med. Biol.* **50** 5175
[6] Yu K, shao Q, Ashkenazi S, Bischof J C and He B 2016 *IEEE Trans. Med. Imaging* **35** 2301
[7] He W, Liu G, Zhang Y and Zeng X P 2010 *Conf. Proc.*

IEEE Eng. Med. Biol. Soc. **2010** 4983
[8] Ammari H, Boulmier S and Millien P 2015 *Mathematics* **259** 5379
[9] Hu G, Li X and He B 2010 *Appl. Phys. Lett.* **97** 103705
[10] Huang X, Liu G and Xia H 2014 *Adv. Mater. Res.* **756** 4677
[11] Li Y L, Liu Z B, Ma Q Y, Guo X S and Zhang D 2010 *Chin. Phys. Lett.* **27** 084302
[12] Chen X Z, Ma Q Y, Zhang F, Sun X D and Cui H C 2012 *Chin. Phys. Lett.* **29** 097203
[13] Han W, Shah J and Balaban R S 1998 *IEEE Trans. Biomed. Eng.* **45** 119
[14] Xu Y, Haider S and Hrbek A 2007 *IFMBE Proc.* **17** 292
[15] Haider S, Hrbek A and Xu Y 2008 *Physiological Meas.* **29** S41
[16] Zeng X P, Liu G Q, Xia H and Xu X 2010 *Proc. 2010-Int. Conf. Biomed. Eng. Inf. BMEI.* **1** 95
[17] Kunyansky L 2012 *Inverse Probl.* **28** 35002
[18] Guo L, Liu G Q, Xia H and Chen J 2013 *Chin. Phys. Lett.* **30** 124303
[19] GraslandMongrain P, Mari J M, Chapelon J Y and Lafon C 2013 *IRBM* **34** 357
[20] Guo L, Liu G Q, Xia H, Liu Y and Lu M H 2014 *Chin. Phys.* B **23** 104303
[21] Guo L, Liu G F, Yang Y J and Liu G Q 2015 *Chin. Phys. Lett.* **32** 094301
[22] Zengin R and Gençer N G 2016 *Phys. Med. Biol.* **61** 5887
[23] Robert P, Ito M and Takahasi T 1992 *IEEE Trans. Magn.* **28** 1166
[24] Lin Q H and Li B M 2010 *Nanjing Li Gong Daxue Xuebao* **34** 217 (in Chinese)
[25] Cui X, Li S, Feng H and Li G 2017 *J. Comput. Phys.* **336** 192
[26] Soleimani M and Lionheart W R B 2006 *IEEE Trans. Med. Imaging* **25** 1521
[27] O'Brien K, Daducci A, Kickler N, lazeyras F, Gruetter R, Feiweier T and Krueger G 2013 *IEEE Trans. Med. Imaging* **32** 1515
[28] Morisue T 1982 *IEEE Trans. Magn.* **18** 531
[29] He B 2005 *Conf Proc. IEEE Eng. Med. Biol. Soc.* **4** 4178
[30] Zhang S, Zhang X Y, Wang H B, Zhao M K, Li Y, Xu G Z and Yan W L 2016 *IEEE Trans. Magn.* **52** 1
[31] Guo G P, Ding H P, Dai S J and Ma Q Y 2017 *Chin. Phys.* B **26** 084301